



Cite this: *Nanoscale*, 2016, **8**, 3510

Distinct CPT-induced deaths in lung cancer cells caused by clathrin-mediated internalization of CP micelles†

Yu-Sheng Liu,^{‡,a,b} Ru-You Cheng,^{‡,b} Yu-Lun Lo,^b Chin Hsu,^c Su-Hwei Chen,^a Chien-Chih Chiu^{*d} and Li-Fang Wang^{*b,e}

We previously synthesized a chondroitin sulfate-*graft*-poly(ϵ -caprolactone) copolymer (H-CP) with a high content of poly(ϵ -caprolactone) (18.7 mol%), which self-assembled in water into a rod-like micelle to encapsulate hydrophobic camptothecin (CPT) in the core (micelle/CPT) for tumor-targeted drug delivery. As a result of the recognition of the micelle by CD44, the micelle/CPT entered CRL-5802 cells efficiently and released CPT efficaciously, resulting in higher tumor suppression than commercial CPT-11. In this study, H1299 cells were found to have a higher CD44 expression than CRL-5802 cells. However, the lower CD44-expressing CRL-5802 cells had a higher percentage of cell death and higher cellular uptake of the micelle/CPT than the higher CD44-expressing H1299 cells. Examination of the internalization pathway of the micelle/CPT in the presence of different endocytic chemical inhibitors showed that the CRL-5802 cells involved clathrin-mediated endocytosis, which was not found in the H1299 cells. Analysis of the cell cycle of the two cell lines exposed to the micelle/CPT revealed that the CRL-5802 cells arrested mainly in the S phase and the H1299 cells arrested mainly in the G2-M phase. A consistent result was also found in the evaluation of γ -H2AX expression, which was about three-fold higher in the CRL-5802 cells than in the H1299 cells. A near-infrared dye, IR780, was encapsulated into the micelle to observe the *in vivo* biodistribution of the micelle/IR780 in tumor-bearing mice. The CRL-5802 tumor showed a higher fluorescence intensity than the H1299 tumor at any tracing time after 1 h. Thus we tentatively concluded that CRL-5802 cells utilized the clathrin-mediated internalization pathway and arrested in the S phase on exposure to the micelle/CPT; all are possible reasons for the better therapeutic outcome in CRL-5802 cells than in H1299 cells.

Received 26th November 2015,
 Accepted 6th January 2016

DOI: 10.1039/c5nr08345a
www.rsc.org/nanoscale

Introduction

Chondroitin sulfate (CS) is a natural polysaccharide and has many merits, such as biocompatibility, biodegradability,¹ and anti-inflammatory properties;² in addition, it is a natural

ligand for the cluster determinant (CD44) receptor.³ The CD44 receptor is one of the membrane receptors that is over-expressed on many solid tumor surfaces.^{4,5} Thus CS can be used as a specific molecular ligand for targeting cancer cells through CD44-mediated endocytosis.³

A copolymer (CP) based on CS and polycaprolactone (PCL) has been synthesized as a carrier for anticancer drugs.⁶ Both CS and PCL are FDA-approved nontoxic materials. As a result of its amphiphilic properties, the CP copolymer can self-assemble into micelles in water, which can then be utilized to encapsulate a hydrophobic anticancer drug, camptothecin (CPT), in the core for tumor-targeted delivery. CPT is an anti-neoplastic agent, but has low aqueous solubility and only short-term stability of the lactone ring structure, which have limited its development in clinical settings.^{7,8} The advantages of using the CP self-assembled micelles in drug-delivery systems include not only recognition by CD44, but also preservation of the lactone ring of CPT in the blood circulation.⁹

^aSchool of Pharmacy, Kaohsiung Medical University, Kaohsiung 807, Taiwan

^bDepartment of Medicinal and Applied Chemistry, College of Life Science, Kaohsiung Medical University, Kaohsiung 807, Taiwan

^cDepartment of Physiology, Faculty of Medicine, College of Medicine, Kaohsiung Medical University, Kaohsiung 807, Taiwan

^dDepartment of Biotechnology, College of Life Science, Kaohsiung Medical University, Kaohsiung 807, Taiwan

^eInstitute of Medical Science and Technology, National Sun Yat-Sen University, Kaohsiung 804, Taiwan. E-mail: lfwang@kmu.edu.tw; Fax: +886-7-3125339; Tel: +886-7-3121101-2217

†Electronic supplementary information (ESI) available. See DOI: 10.1039/c5nr08345a

‡Equal contribution.

A polysaccharide-modified nanoparticle prevents recognition by the reticuloendothelial system,^{9,10} similar to the role of poly(ethylene glycol).

The physicochemical properties of the micelle and the CPT-loaded micelle (micelle/CPT) were thoroughly characterized and the therapeutic efficacy of the micelle/CPT was demonstrated in non-small-cell lung cancer (NSCLC) CRL-5802 cells expressing the CD44 receptor on the cell surface.⁶ The intensity of CD44 expression on the surface of several NSCLC cell lines was examined and H1299 cells were found to have the highest expression of CD44. When exposed to the micelle/CPT, the higher CD44-expressing H1299 cells showed lower cytotoxicity and apoptosis than the lower CD44-expressing CRL-5802 cells. To account for the higher therapeutic efficacy of CRL-5802 cells, experiments were conducted using chemical inhibitors of endocytosis to understand whether the internalization of the micelle/CPT involved different pathways in the two cell lines and how this affected cell cycle arrest, apoptosis, and γ -H2AX formation. The *in vivo* biodistribution of the micelle in tumor-bearing mice was examined using near-infrared (IR) optical imaging to determine the amount of micelles accumulated in the two tumors.

Materials and methods

Materials

Copper(i) bromide (CuBr), 3-(4,5-dimethyl-thiazol-2-yl)-2,5-diphenyl-tetrazolium bromide (MTT), propidium iodide (PI), sodium borate, Tween 20, dimethyl sulfoxide-*d* (DMSO-*d*₆), chloroform-*d* (CDCl₃), and deuterium oxide (D₂O) were purchased from Aldrich (St Louis, MO, USA). 2,2'-Bipyridine, 2-bromo-2-methylpropionyl bromide, Amberlite IR120, and Dowex 50W×8 (H) were purchased from Acros (Morris Plains, NJ, USA). Chondroitin sulfate-*g*-poly(ϵ -caprolactone) copolymer containing a high content of poly(ϵ -caprolactone) (H-CP) and Rhodamine 123-conjugated H-CP (Rh123-H-CP) were prepared as described previously.⁶ Camptothecin (CPT) was acquired from the Industrial Technology Research Institute of Taiwan. Bovine serum albumin (BSA) was purchased from MDBio Inc. (Taipei, Taiwan). Fetal bovine serum (FBS) was purchased from Biological Industries (Beit Haemek, Israel). Dulbecco's modified Eagle's medium (DMEM) and Tris-glycine gels were purchased from Invitrogen (Carlsbad, CA, USA). An annexin V-FITC apoptosis detection kit was purchased from Strong Biotech (Taipei, Taiwan). For the western blot assay, the primary antibodies against XIAP, γ -H2AX, and β -actin were purchased from Santa Cruz Biotechnology (Santa Cruz, CA, USA) and primary antibodies against p27^{Kip1}, CDK2, and cyclin A were purchased from GenTex (Irvine, CA, USA).

Preparation of H-CP micelles

An H-CP copolymer was synthesized as reported previously.⁶ The H-CP micelle was prepared by a simple dialysis method. Briefly, the H-CP copolymer (10 mg) was dispersed in 5 mL of DMSO containing 4 μ L of trifluoroacetic acid at 60 °C. The

solution was placed in a dialysis bag (M_w cut-off 1000 membrane, Spectrum Labs, Rancho Dominguez, CA, USA) and dialyzed against DD water for 1 day, followed by freeze-drying to produce the micellar product.

CPT or IR780-encapsulated micelles (micelle/CPT or micelle/IR780)

The method for preparing CPT- or IR780-loaded micelles was similar to that for preparing the H-CP micelle. In brief, CPT or IR780 powder was dissolved in DMSO at 1 mg mL⁻¹ to yield a stock solution. The H-CP (10 mg) powder was dissolved in 5 mL of DMSO containing 4 μ L of trifluoroacetic acid at 60 °C, followed by the addition of 1 mL of the CPT or IR780 stock solution. The solution was dialyzed against DD water using an M_w cut-off 6000 membrane (Spectrum Labs) for 1 day and then filtered to remove the unencapsulated CPT or IR780. Finally, the micelle/CPT or micelle/IR780 was obtained by freeze-drying.

Cell lines

CRL-5802 and H1299 (NSCLC) cell lines were obtained from Dr Cheng at the Biomedical Science and Environmental Biology, Department of Kaohsiung Medical University in Taiwan and cultured in DMEM supplemented with 10% FBS and 1% penicillin-streptomycin at 37 °C under humidified 5% CO₂.

Expression of CD44 receptor

An immuno-phenotype analysis was used to evaluate the expression of the CD44 receptor in several cell lines.¹¹ The cells (5 \times 10⁵ cells per tube) were suspended with 90 μ L of PBS in 1.5 mL Eppendorf tubes and 10 μ L of CD44-FITC (50 μ g mL⁻¹) (eBioscience, San Diego, CA, USA) were added and co-incubated at 4 °C for 30 min in the dark. The cells were washed three times with 0.1 M PBS and resuspended in 1 mL of PBS. The fluorescence intensity of FITC was measured using flow cytometry (Becton-Dickinson, Mansfield, MA, USA). The data were averaged from three experiments.

Cytotoxicity

The cytotoxicities of CPT and micelle/CPT were measured using the MTT assay. The CPT powder was dissolved in DMSO to give a stock solution (2 mg mL⁻¹), followed by dilution to a concentration of 0.0025–5.0 μ g mL⁻¹ in DMEM containing 10% FBS for cytotoxicity testing of CPT. The equivalent CPT concentration of the micelle/CPT was controlled within 0.0025–5.0 μ g mL⁻¹. Cells were seeded in 96-well culture plates at a density of 5 \times 10³ cells per well in DMEM containing 10% FBS for 24 h. The culture medium was replaced with 100 μ L of medium containing various concentrations of CPT. After 24 h the cells were washed three times with 0.1 M PBS and replenished with fresh medium to post-incubate for another 24 or 48 h. The number of viable cells was measured by estimating their mitochondrial reductase activity using the tetrazolium-based colorimetric method.

Intracellular uptake and inhibition of endocytosis

The synthesis of rhodamine 123-conjugated H-CP (Rh123-H-CP) was carried out as reported previously.⁶ The cellular uptake of Rh123-H-CP was studied using a flow cytometer. CRL-5802 or H1299 cells were seeded at a density of 2×10^5 cells per well in six-well plates in DMEM supplemented with 10% FBS and incubated for 24 h. The culture medium was removed and replaced with 2 mL of DMEM containing Rh123-H-CP (100 $\mu\text{g mL}^{-1}$). The cells containing Rh123-H-CP were incubated at 37 °C for another 30 min or 2 h. The cells were washed three times with 0.1 M PBS, collected, and analyzed using the flow cytometer.

Three chemical inhibitors were utilized to study the endocytosis pathways using the following concentrations: wortmannin (50 nM), chlorpromazine (0.5, 1.0, 5.0, and 10 $\mu\text{g mL}^{-1}$), and genistein (50, 100, and 200 μM).¹² CRL-5802 or H1299 cells were seeded at a density of 1×10^5 cells per well in six-well plates in DMEM supplemented with 10% FBS and incubated for 24 h. The cells were pretreated with various concentrations of inhibitors at 37 °C for 30 min. Next, the cells were washed and replaced with 2 mL of DMEM containing Rh123-H-CP (100 $\mu\text{g mL}^{-1}$). The cells were further incubated at 37 °C for 2 h, washed three times with 0.1 M PBS, collected and then analyzed using flow cytometry.

Cell cycle analysis

The effects of CPT and micelle/CPT internalization on the progression of the cell cycle of cancer cells were studied by cell cycle analysis. Cells (CRL-5802 or H1299) were seeded at a density of 2×10^5 cells per well in six-well plates and incubated in DMEM supplemented with 10% FBS for 24 h. Subsequently, CPT or micelle/CPT were added to the cells at an equivalent CPT concentration of 0.1 $\mu\text{g mL}^{-1}$ in the same culture medium. The cells containing the drug were then incubated at 37 °C for 24 h. The culture media were removed and the cells were washed and detached using 0.1% 1× trypsin (1 mL per well). The cells were collected by centrifugation at 1000 rpm for 5 min and fixed overnight using 70% ethanol. Following fixation, the cells were washed and incubated with 20 $\mu\text{g mL}^{-1}$ PI and 20 $\mu\text{g mL}^{-1}$ RNase in 0.1 M PBS at room temperature for 15 min. Cell pellets were obtained by centrifugation at 1000 rpm for 5 min and were then resuspended in 0.1 M PBS to determine the distribution of the cells in various stages of the cell cycle using flow cytometry.

Cell apoptosis

To estimate the apoptosis-inducing efficiency of CPT and micelle/CPT, the annexin-V/PI dual-staining assay was utilized. The cells were plated at a density of 2×10^5 cells per well into six-well culture plates and incubated in DMEM containing 10% FBS for 24 h. Next, the cells were treated with CPT or micelle/CPT at a CPT concentration of 0.1 $\mu\text{g mL}^{-1}$ in DMEM without 10% FBS at 37 °C for 24 h. The H-CP micelle and cultured cells were used as blank and control groups, respectively. The cells were washed three times with 0.1 M PBS, collected,

and then labeled with annexin-V-FITC (10 $\mu\text{g mL}^{-1}$) and PI (20 $\mu\text{g mL}^{-1}$) at 37 °C for 30 min. After labeling, the cells were analyzed using flow cytometry. The experiment was repeated three times.

Evaluation of γ -H2AX activation

The degree of DNA damage was assessed using γ -H2AX as a marker.¹³ Cells were seeded at a density of 2×10^5 cells per well in six-well tissue culture plates and incubated in DMEM medium containing 10% FBS for 24 h. CPT or micelle/CPT was added to the culture medium at a CPT concentration of 0.1 $\mu\text{g mL}^{-1}$ and then incubated at 37 °C for 24 h. The cells were washed and harvested using 0.1% 1× trypsin (1 mL per well), collected in Eppendorf tubes, and centrifuged at 3000 rpm for 10 min. Next, 70% ethanol was added dropwise into the tubes to fix the cells at -20 °C overnight. After fixation, the cells were washed in BSA-T-PBS solution (1% bovine serum albumin and 0.2% Triton X-100 in PBS; Sigma) and incubated overnight with 100 mL of the BSA-T-PBS solution containing 0.2 mg *p*-histone H2AX (Ser 139) monoclonal antibody (#sc-101696, Santa Cruz Biotechnology) on a shaker at 4 °C. Following centrifugation, the supernatant was discarded from the tubes and the residue was washed twice in the BSA-T-PBS solution. Alexa Fluor 488-tagged secondary antibody (Jackson Laboratory, Bar Harbor, ME, USA) was diluted 1:200 with the BSA-T-PBS solution and mixed with the cells at 37 °C for 1 h. After two washes with the BSA-T-PBS solution, the cells were incubated with 20 $\mu\text{g mL}^{-1}$ PI at room temperature for 30 min. The fluorescent intensity of the cells was recorded using flow cytometry.

Western blot analysis

CRL-5802 or H1299 cells were plated at a density of 2×10^5 cells per well into six-well culture plates and incubated in DMEM (1 mL) containing 10% FBS for 24 h. The cells were treated with CPT or micelle/CPT at a CPT concentration of 0.1 $\mu\text{g mL}^{-1}$ at 37 °C for 1 h. The cells were scraped and collected into 1.5 mL Eppendorf tubes and proteins were extracted from the cells by mixing with lysis buffer (0.05 mol L^{-1} Tris-HCl at pH 6.8, 2% SDS, and 6% β -mercaptoethanol) in ice for 30 min. Following lysis, the supernatant solution was separated from the cell pellets by centrifugation at 13 000 rpm for 30 min and the protein concentration was measured using a BCA protein assay kit (Pierce, Rockford, IL, USA). Next, each protein (30 μg) was mixed with a 5× sample dye followed by boiling at 95 °C for 5 min. An equal amount of protein (30 μg) was separated using 10% SDS-PAGE gel and transferred to a polyvinylidene difluoride (PVDF) membrane (Merck Millipore Life Science, Darmstadt, Germany). The PVDF membrane was blocked in blocking buffer (5% nonfat milk powder dissolved in Tris-buffered saline containing 0.1% Tween 20 (TBST)) at room temperature. Following 1 h of incubation, the blocked PVDF membrane was probed at 4 °C overnight with a 1:1000 dilution of phosphorylated histone H2AX, γ -H2AX (Ser 139) primary antibody in 1% nonfat milk-TBST buffer. The next day, the PVDF membrane

was washed three times with TBST and incubated with a 1:4000 dilution of a horseradish peroxidase-conjugated secondary antibody (Thermo Fisher Scientific, San Jose, CA, USA) in TBST at room temperature for 1 h. The PVDF membrane was washed three times with TBST and developed using an enhanced chemiluminescence detection kit (Amersham, Piscataway, NJ, USA).

Confocal laser scanning microscopy

CRL-5802 or H1299 cells were seeded at a density of 1×10^5 cells per well in 12-well plates (containing one glass coverslip per well) in DMEM supplemented with 10% FBS for 24 h. The culture medium was replaced with 1 mL of medium without 10% FBS, which contained either CPT or micelle/CPT at a CPT concentration of $0.1 \mu\text{g mL}^{-1}$. The H-CP micelle (blank) and cultured cells were used as control groups. The cells with or without CPT were incubated at 37°C for 24 h. The coverslips containing the cells were removed, washed gently twice with PBS, and then treated with 4% paraformaldehyde for 30 min to fix the cells. After fixing, the cells on the coverslips were washed twice with PBS and then incubated with blocking buffer (1% BSA in PBS) at room temperature for 15 min. The supernatant was removed and then the cells were mixed with *p*-histone H2AX (Ser 139) monoclonal primary antibody (dilution 1:300 with blocking buffer) at room temperature. After standing for 1 h, the cells on the coverslips were washed three times with blocking buffer and stained with Alexa Fluor 488-tagged secondary antibody, which was diluted to 1:200 with the blocking buffer and incubated at 37°C for 1 h. After two washes with the blocking buffer, the coverslips containing the cells were mounted with Fluoromount-G (eBioscience) for CLSM observation (Olympus Fv 1000, Tokyo, Japan).

In vivo biodistribution

Nude mice (Balb/cAnN.Cg-Foxn1^{nu}/CrlNarl, male, about 6 weeks old) were purchased from the National Laboratory Animal Center of Taiwan. The animal experiment was approved by the Institutional Animal Care and Use Committee of Kaohsiung Medical University. The biodistribution of the micelle/IR780 was monitored by non-invasive fluorescence in tumor-bearing mice with two tumors grafted on the right (H1299) and left (CRL-5802) hind legs. After the tumors had grown to approximately 150 mm^3 in volume, the micelle/IR780 (1.75 mg kg^{-1} of IR780) was intravenously injected into tumor-bearing mice *via* the lateral tail vein.¹⁴ Following the injection, the micelle/IR780 was imaged at several time points (1, 4, 8, 12, 24, 36, and 48 h) using an IVIS Spectrum System 3D (Caliper Life Sciences, Hopkinton, MA, USA). The exposure time was set to 2 s and the excitation and emission wavelengths were selected as 745 and 840 nm, respectively, with an ICG filter. After 48 h, the relevant organs, tissues, and tumors were harvested from the mice and imaged immediately to quantify their intensities using the region of interest function of the Living Image software. The heart, liver, and kidney were

sectioned into slices for histopathological examination with hematoxylin and eosin (H&E) staining.

Statistical analysis

Mean and standard deviation (SD) values of the data were calculated. The comparison between groups was tested using Student's *t*-test and $P < 0.05$ was considered to be significant.

Results and discussion

CD44 expression and cytotoxicity

A chondroitin sulfate-*g*-poly(ϵ -caprolactone) copolymer with a high content of PCL (18.7 mol%) (H-CP) was synthesized and used to encapsulate the hydrophobic CPT (micelle/CPT) in its core for tumor-targeted delivery.⁶ With recognition of the H-CP micelle by CD44, the micelle/CPT entered the CRL-5802 cells and released the CPT efficaciously, showing higher tumor suppression than commercial CPT-11. Examination of the CD44 expression on the surface of many NSCLCs revealed that the H1299 cells showed a higher CD44 expression than the CRL-5802 cells (Fig. 1). Thus it was hypothesized that the therapeutic outcome using CPT released from the micelle/CPT against the H1299 cells should be better than that against the CRL-5802 cells.

To test this hypothesis, the cell viabilities of the two cell lines exposed to free CPT and the micelle/CPT were promptly screened after 24 and 48 h of incubation (Fig. 2). The cytotoxicity of the micelle/CPT was higher than that of free CPT in both cell lines and after both durations of incubation. Encapsulated nanoparticles of anticancer drugs usually have advantages over their parent drugs including: (1) an increase in the water solubility of poorly soluble or insoluble anticancer drugs and an enhancement in their biodistribution and therapeutic efficacy; (2) an accumulation of anticancer drugs in tumor tissues by the enhanced permeation and retention (EPR) effect and a reduction in systemic side-effects; and (3) protection of the anticancer drugs against deactivation during blood circulation, transport to targeted organs or tissues, and intracellular trafficking. In the CRL-5802 cells, the micelle/CPT showed a higher potency in cell-killing activity ($\text{IC}_{50} = 0.01 \mu\text{g mL}^{-1}$ for 24 h, $\text{IC}_{50} = 0.004 \mu\text{g mL}^{-1}$ for 48 h) than in the H1299 cells ($\text{IC}_{50} = 1.36 \mu\text{g mL}^{-1}$ for 24 h, $\text{IC}_{50} = 0.15 \mu\text{g mL}^{-1}$ for 48 h). This result completely contradicted the hypothesis that the higher CD44 expression on H1299 cell membrane should enhance the cellular uptake of the micelle/CPT, leading to a better therapeutic outcome for CPT.

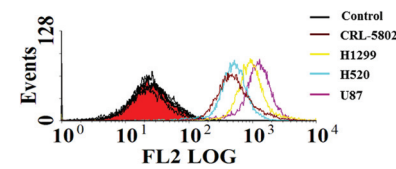


Fig. 1 Fluorescence intensities of CD44 expression in non-small-cell lung cancer cell lines and U87 cells (a human glioblastoma cell line).

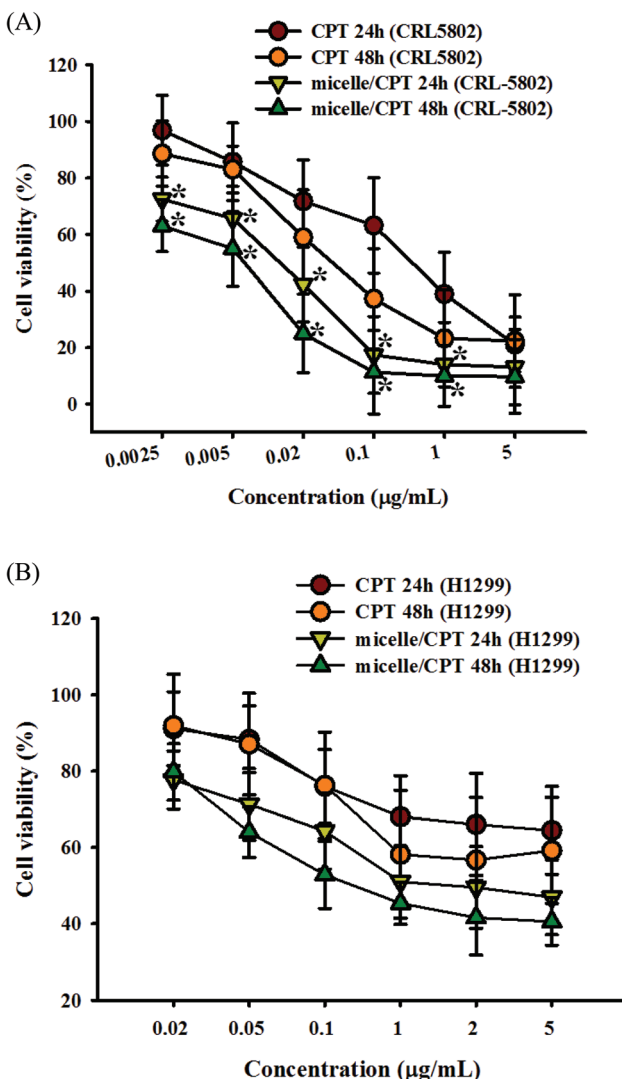


Fig. 2 Cell viability tests using an MTT assay for CPT and CPT-loaded micelles (micelle/CPT) against (A) CRL-5802 cells and (B) H1299 cells for 24 and 48 h of incubation.

Intracellular uptake and inhibition of endocytosis

To further confirm the hypothesis, flow cytometry was utilized as an alternative measurement to examine the internalization efficacy of the H-CP micelle into two cell lines. A fluorescent dye, rhodamine 123 (Rh123), was conjugated to the micelle. As seen in Fig. 3A and B, the cellular uptake of the Rh123-H-CP micelle into the CRL-5802 cells was much higher than that into H1299 for both 30 min and 2 h of incubation. This result agreed with the cytotoxicity finding (Fig. 2). The higher CD44-expressing H1299 cells were less able to internalize the micelle, which may be attributed to pathways that were involved in the uptake of the micelle in the two cell lines other than CD44-mediated endocytosis.

Different endocytosis pathways involved in cellular uptake in nanomedicine have been widely reported.¹⁵ The cells were therefore pretreated with three chemical inhibitors before

being treated with the Rh123-H-CP micelle. Wortmannin was selected for macropinocytosis, chlorpromazine for clathrin-mediated endocytosis (CME), and genistein for caveolae-mediated endocytosis.⁶ The inhibition effect of these three inhibitors on the cellular uptake of the micelle was preliminarily tested at the following concentrations: 50 nM wortmannin, 10 μ g mL⁻¹ chlorpromazine, and 200 μ M genistein. Flow cytometric diagrams showed a left shift when the CRL-5802 and H1299 cells were pretreated with chlorpromazine and genistein, respectively, indicating the inhibition effect, whereas the diagrams remained intact when the cells were treated with wortmannin (Fig. S1†). Thus the dose-dependent inhibition of chlorpromazine and genistein was further tested. Flow cytometric diagrams showed an apparent shift to the left compared with the control group when the CRL-5802 cells were pretreated with chlorpromazine at 5 and 10 μ g mL⁻¹ and genistein at 100 and 200 μ M (Fig. S1†). Subsequently, the cellular accumulation of fluorescence intensity was quantified according to the control group. The fluorescence intensity decreased significantly for the chlorpromazine- and genistein-pretreated cells at the reported concentrations (Fig. 3C). The same test was performed on H1299 cells. No inhibition effect was observed in H1299 cells pretreated with different doses of chlorpromazine. In contrast, there was an apparent shift to the left when the cells were pretreated with genistein at a low dose of 10 μ M (Fig. S1† and Fig. 3D). The flow cytometric results suggested that the cellular uptake of the micelle was dependent on the cell line. The cellular uptake of the micelle into CRL-5802 cells utilized CD44-, clathrin-, and caveolae-mediated endocytosis; in the H1299 cells, however, only CD44- and caveolae-mediated endocytosis pathways were involved.

Cellular internalization and the subsequent intracellular processing of nanoparticles are key barriers to the successful *in vitro* and *in vivo* delivery of drugs. Clathrin- and caveolin-dependent endocytosis have been extensively studied.¹⁵ Clathrin-dependent endocytosis yields acidified vesicles (pH 5–6) that fuse with lysosomes (about pH 4.5). Caveolin-dependent uptake is less well characterized, but is associated with the formation of caveosomes that are less acidified and are believed to avoid trafficking to lysosomes. The differences in endocytic vesicles and subsequent processing may significantly impact the intracellular destination of drug-encapsulated nanoparticles. There are several examples in which CME appears to be defined as the most prominent mechanism for cellular entry.^{16–20} For example, nanoparticles of D,L-poly(lactide) (PLA) and poly(ethylene glycol-co-lactide) (PEG-co-PLA) have been explored for drug delivery. As a result of the presence of the partially hydrolyzed PLA, the surface of the nanoparticles was negatively charged and usually altered with cationic surfactants such as stearylamine.^{16,21} In the polarized MDCK epithelial cells, the nanoparticles used CME independent of their charge. In contrast, in non-polarized HeLa cervical cancer cells, the anionic particles used multiple pathways (CME and caveolae-mediated), whereas the cationic particles appeared to be restricted to CME and macropinocytosis. Hyaluronic acid (HA) conjugated with hydrophobic poly(L-histidine) (PHis) was

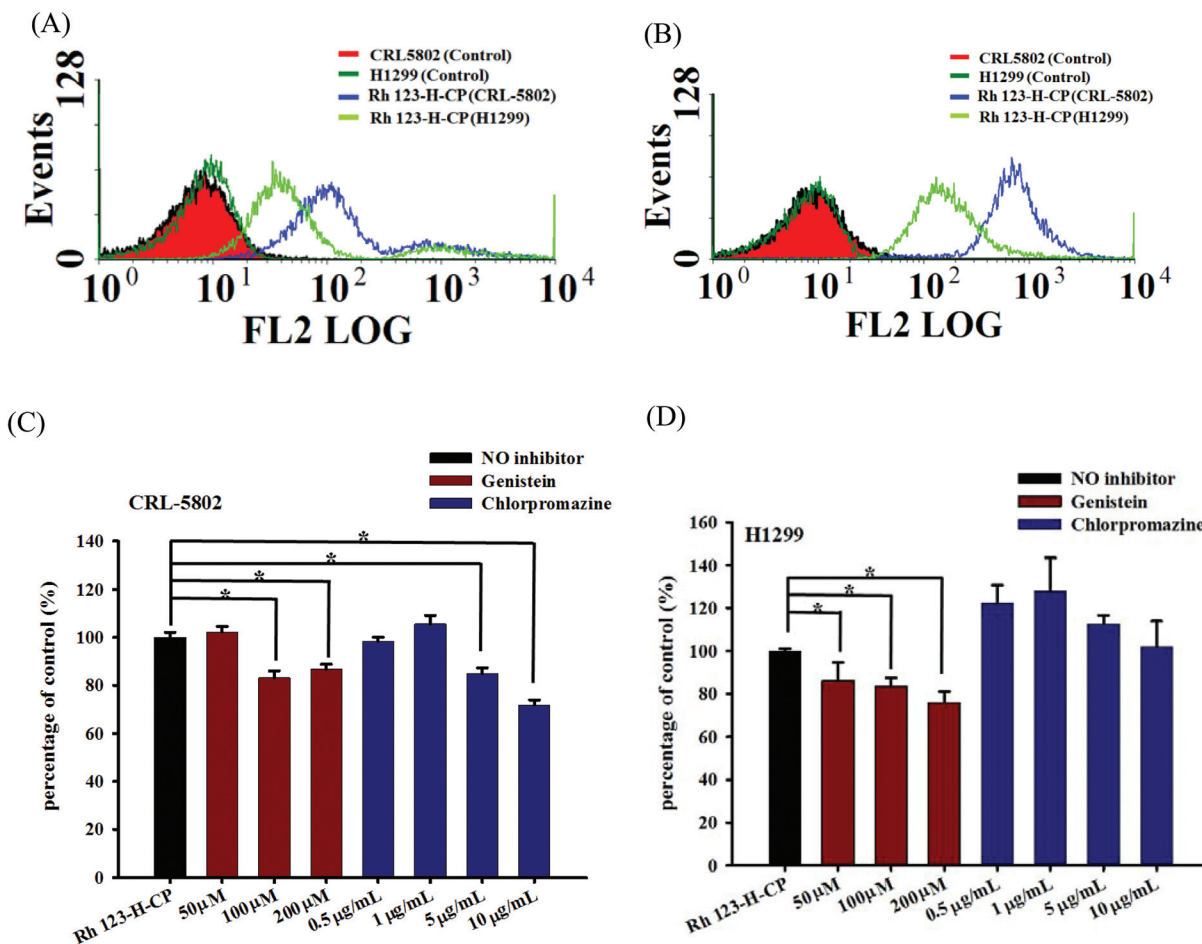


Fig. 3 Flow cytometric histograms of CRL-5802 and H1299 cells exposed to Rh123-linked micelle for (A) 30 min and (B) 2 h of incubation. The inhibition of intracellular uptake in (C) CRL-5802 cells and (D) H1299 cells pretreated with dose-dependent chlorpromazine and genistein inhibitors for 30 min. before the cells were exposed to the micelle for 2 h of incubation.

used to prepare a pH-responsive and tumor-targeted copolymer, hyaluronic acid-g-poly(L-histidine) (HA-PHis), for use as a carrier for anticancer drugs.²² The results showed that the pH-responsive HA-PHis micelles were taken up *via* CD44 receptor-mediated endocytosis as well as *via* CME and were delivered to the lysosomes, which contributed to triggering the release of doxorubicin into the cytoplasm. A review of these examples showed that using the CME pathway seems to enhance the cellular uptake of biodegradable micelles and results in better therapeutic outcomes.

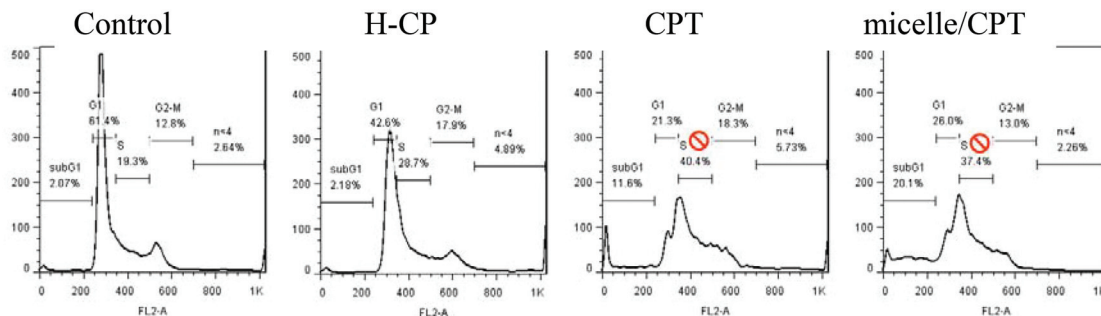
Cell cycle

CPT is a potent anticancer drug that inhibits DNA topoisomerase I and causes the apoptosis of cancer cells.²³ To understand further the mechanism of drug action, the effect of CPT on the cell cycle of two cell lines was evaluated. Cell cycle arrest was analyzed using PI-labeled RNase in CRL-5802 and H1299 cells after 24 h of post-incubation. Flow cytometric analysis showed 21.3, 40.4, and 18.3% of arrest for CPT-treated CRL-5802 cells and 26.0, 37.4, and 13.0% of arrest for

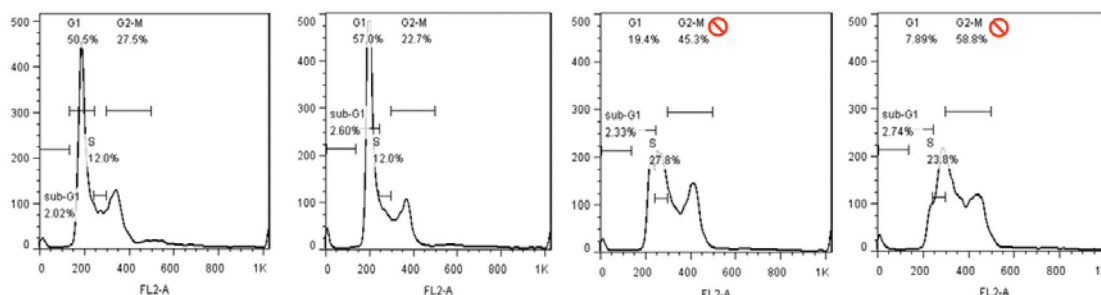
micelle/CPT-treated CRL-5802 cells in the G₁, S and G₂-M phases, respectively (Fig. 4A). Similarly, flow cytometric analysis was carried out on H1299 cells. There were 19.4, 27.8, and 45.3% of arrest for CPT-treated cells and 7.89, 23.8, and 58.8% for micelle/CPT-treated cells in the G₁, S, and G₂-M phases, respectively (Fig. 4B). Cell cycle analysis revealed that CPT or micelle/CPT arrested mainly CRL-5802 cells in the S phase and H1299 cells in the G₂-M phase. Although CPT has been shown to induce an accumulation of cells at the intra-S phase checkpoint,²⁴ other studies also showed that both low dose CPT and CPT-resistant cancer cells could induce accumulations at the G₁/S transition or G₂/M boundary instead of the intra-S arrest alone.²⁵ This will attenuate the therapeutic outcome of CPT.

The S phase cells of the myelogenous leukemias HL-60 or KG-1 are susceptible to apoptosis in the presence of CPT. However, the glioma cells U-251 MG and D-54 MG, which express ectopic p16, lead to G₁ phase arrest and are resistant to the CPT derivative topotecan.²⁶ In contrast, the human lymphocytic leukemia cells MOLT-4 or mouse L1210 cells are

(A) CRL-5802



(B) H1299



(C)

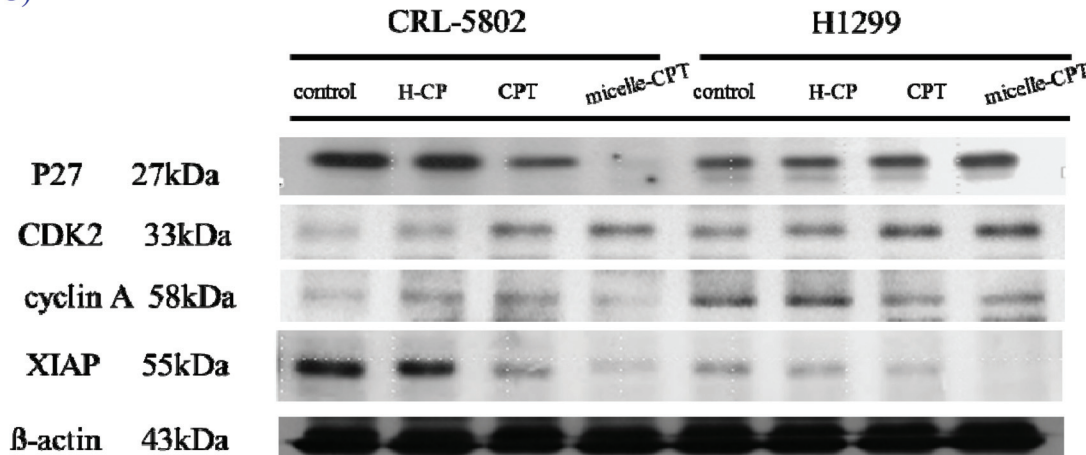


Fig. 4 Cell cycle analysis of H-CP, CPT, and micelle/CPT against (A) CRL-5802 cells and (B) H1299 cells for 24 h of incubation using the equivalent CPT concentration of $0.1 \mu\text{g mL}^{-1}$. (C) Amounts of protein expression of cell cycle modulators p27, CDK2, and cyclin A, and the pro-survival protein XIAP. The results of western blot analysis showed that the micelle/CPT caused a dramatically decreased level of p27 protein in CRL-5802 cells compared with the H1299 cells. β -Actin was used as an internal control for equal loading.

resistant to CPT and no significant CPT-induced accumulation in the S phase was detected.^{27,28} In addition, Goldwasser *et al.*²⁵ showed that the human colon cancer cell lines SW620 and KM12 triggered accumulations in two distinct phases following treatment with CPT. The CPT-resistant KM12 was arrested in G₂, whereas the CPT-sensitive SW620 was irreversibly arrested in the S phase. The effect of CPT on the cell cycle arrest was indeed dependent on the cell line.

The S phase selectivity reflects the formation of double-strand DNA breaks when the advancing replication forks collide with CPT-stabilized topo I-DNA complexes.^{29,30} Additional studies have revealed that further exposure of exponentially growing cells to high CPT concentrations produces a subsequent G₂ arrest in synchronized HeLa cells as a consequence of the impaired activation of cdc2-cyclin B complexes.^{31,32} These results suggested that the alteration in

checkpoints of DNA damage may be a critical factor for defining the chemosensitivity of cancer cells to CPT.

$p27^{kip-1}$ is a member of Cip/Kip family and modulates the progression of the cell cycle by binding cyclin/Cdk complexes. $p27$ acts as a regulator of cell cycle progression at both the G_1/S and S to G_2/M transition phases.³³ In normal cells, $p27$ is a tumor suppressor and has been reported to inhibit progression of the cell cycle. However, the expression of $p27$ has been shown to be a negative indicator that is correlated with the prognosis of patients with oral squamous cancer,³⁴ chronic B-cell lymphocytic leukemia,³⁵ and NSCLC.³⁶ Here, the CPT/micelle causes a dramatic decrease in the level of $p27$ protein in CRL-5802 cells, but not in H1299 cells (Fig. 4C). The down-regulation of $p27$ is presumed to enhance the cytotoxicity of CRL-5802 cells treated with the CPT/micelle.

Cell apoptosis

To examine the induction of cell apoptosis in the CPT-treated or micelle/CPT-treated cells at a CPT concentration of $0.1 \mu\text{g mL}^{-1}$, an annexin-V/PI dual-staining assay was conducted using flow cytometry (Fig. 5A). The four quadrants display necrotic cells stained with PI in the first quadrant (Q1), late apoptotic cells stained with PI and annexin-V in the second quadrant (Q2), early apoptotic cells stained with annexin-V in the third quadrant (Q3), and healthy cells not stained with PI and annexin-V in the fourth quadrant (Q4). The quantification of apoptotic cells is plotted in Fig. 5B. The percentages of late/early apoptotic cells (Q2 + Q3) of micelle/CPT-treated CRL-5802 cells (about 34%) were significantly higher than those of CPT-treated cells (about 25%); however, no significant difference was found in

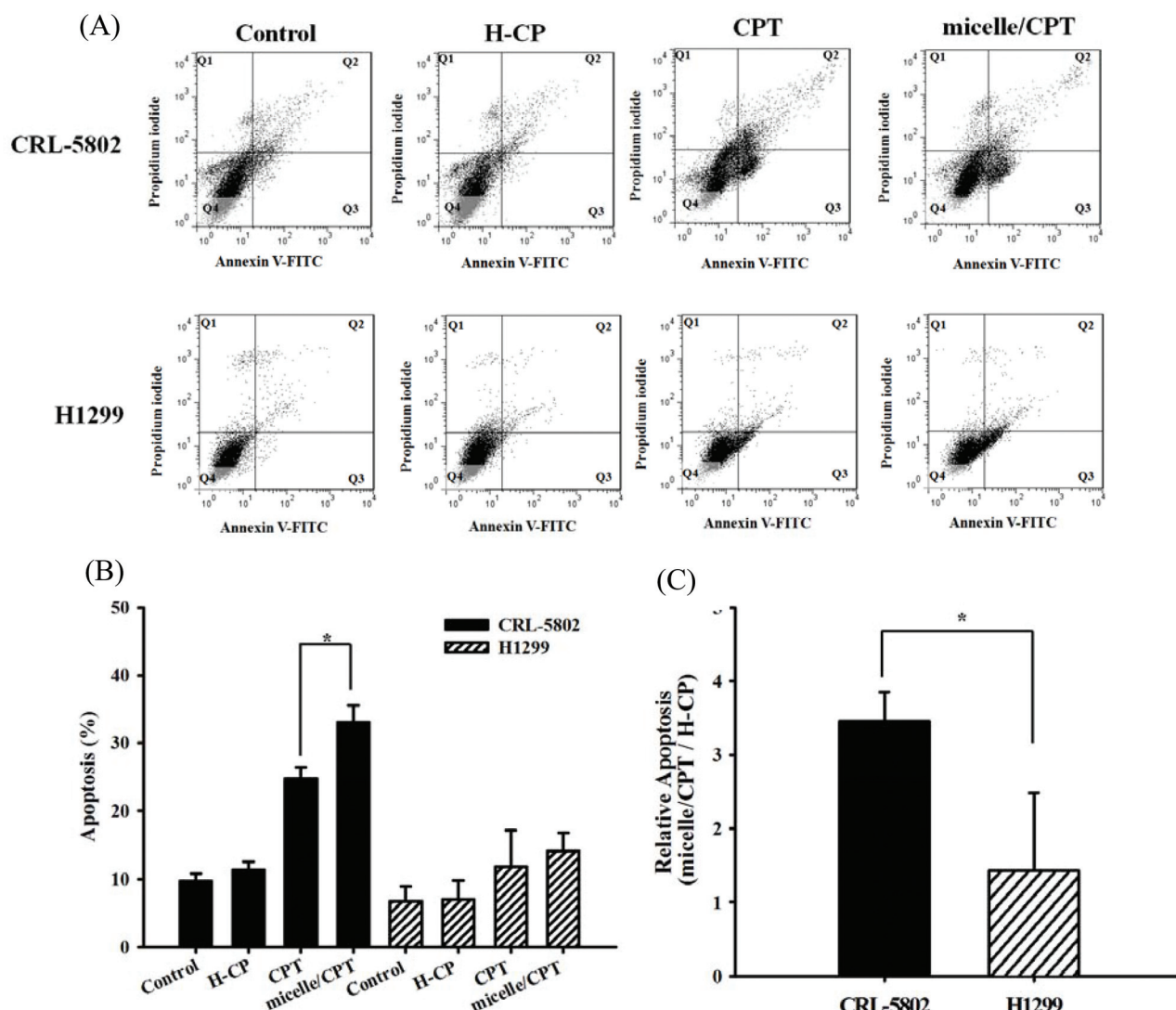


Fig. 5 Induction of apoptosis in CRL-5802 and H1299 cells exposed to H-CP micelle, CPT, and micelle/CPT for 24 h of incubation at 37°C using the equivalent CPT concentration of $0.1 \mu\text{g mL}^{-1}$. (A) Annexin-V/PI dual-staining assay. (B) Percentage of apoptosis cells calculated from (A). (C) Relative apoptosis ratios between cells treated with the micelle/CPT and empty H-CP ($n = 3$, $*P < 0.05$).

H1299 cells exposed to either micelle/CPT or CPT. The relative apoptosis ratios between cells treated with the micelle/CPT and empty H-CP in CRL-5802 and H1299 cells were calculated

and are plotted in Fig. 5C. The relative apoptosis ratio was about 3.5 for CRL-5802 cells and about 1.5 for H1299 cells. These results showed that the micelle/CPT had a significantly

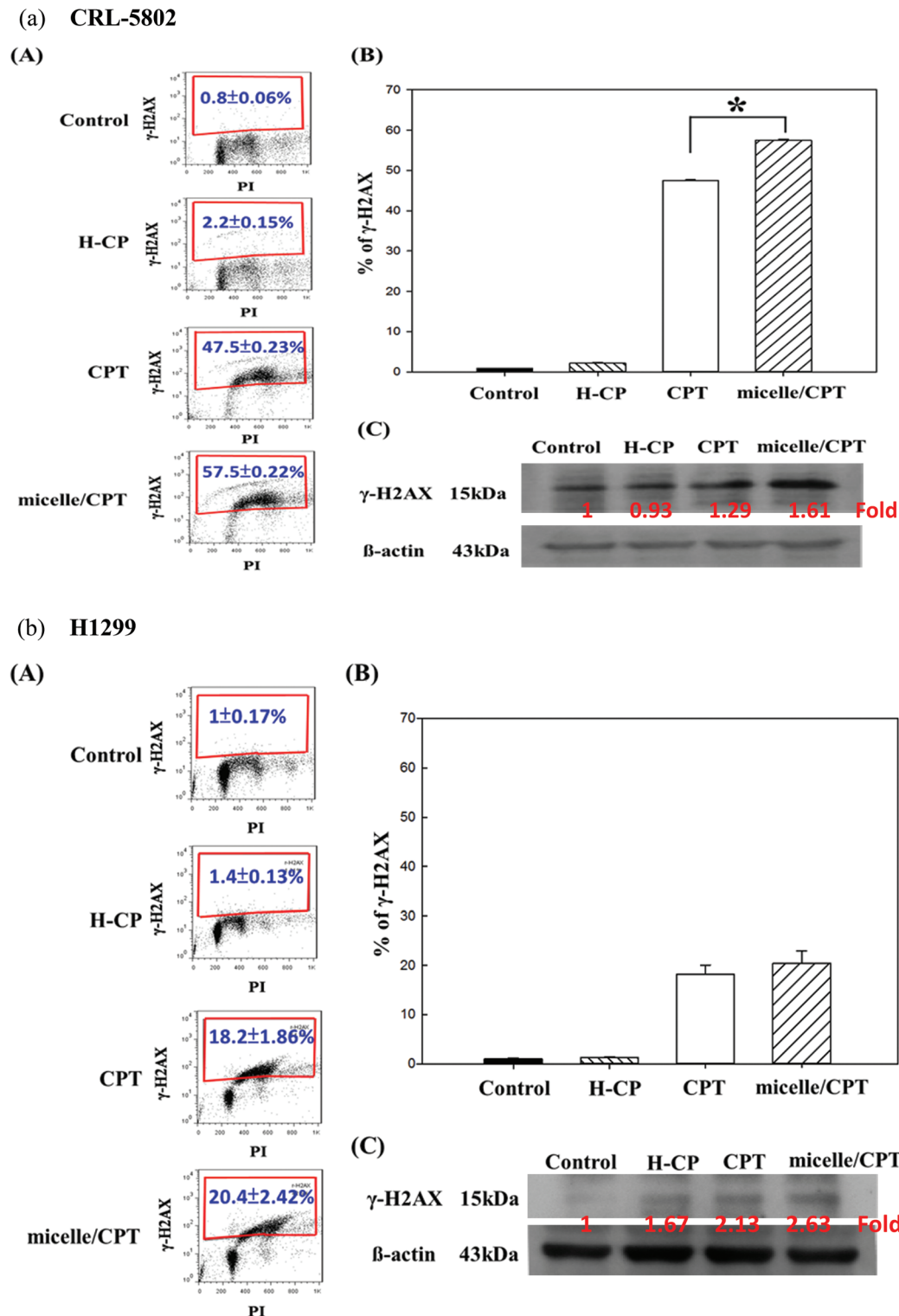


Fig. 6 Formation of γ -H2AX in (a) CRL-5802 cells and (b) H1299 cells exposed to micelle, free CPT, and micelle/CPT for 2 h of incubation using the equivalent CPT concentration of $0.1 \mu\text{g mL}^{-1}$. (A) Expression of γ -H2AX analyzed by flow cytometry, (B) plotted as a percentage of γ -H2AX-positive cells, and (C) by western blotting ($n = 3$, $*P < 0.05$). β -Actin was used as an internal control for equal loading.

higher cell-killing efficiency in CRL-5802 cells than in H1299 cells and that using the micelle/CPT is more potent than using CPT against CRL-5802 cells.

Evaluation of γ -H2AX

The nucleus contains the genomic materials (DNA and RNA), regulates gene expression, and controls the replication of DNA during the cell cycle. Hence damaging the DNA in the nucleus of cancer cells leads to the inhibition of rapid cellular division. The most common assay of DNA fragmentation relies on labeling DNA double-strand breaks with fluorochrome-tagged deoxynucleotides. The induction of double-strand breaks by genotoxic agents provides a signal for histone H2AX phosphorylation on Ser 139; the phosphorylated H2AX is named γ -H2AX. Hence γ -H2AX has evolved as an important biomarker for observing DNA damage.³⁷

To understand the effect of CPT or micelle/CPT on the nucleus of CRL-5802 and H1299 cells, the cells were treated with the equivalent CPT concentration of $0.1 \mu\text{g mL}^{-1}$ for 2 h. The cells were stained with green fluorescent Alexa Fluor 488

Table 1 Summary of *in vitro* data for the two cell lines

		CRL-5802	H1299
CD 44 expression		Low	High
IC ₅₀ (micelle/CPT) ($\mu\text{g mL}^{-1}$)	24 h	0.01	1.36
	48 h	0.004	$0.15 \mu\text{g mL}^{-1}$
Endocytosis pathways		Clathrin and caveolae	Caveolae
Cell cycle		S phase	G ₂ -M phase
Cell apoptosis		33.06 ± 2.49	14.14 ± 2.68
(micelle/CPT) (%)			
γ -H2AX (micelle/CPT)		High	Low

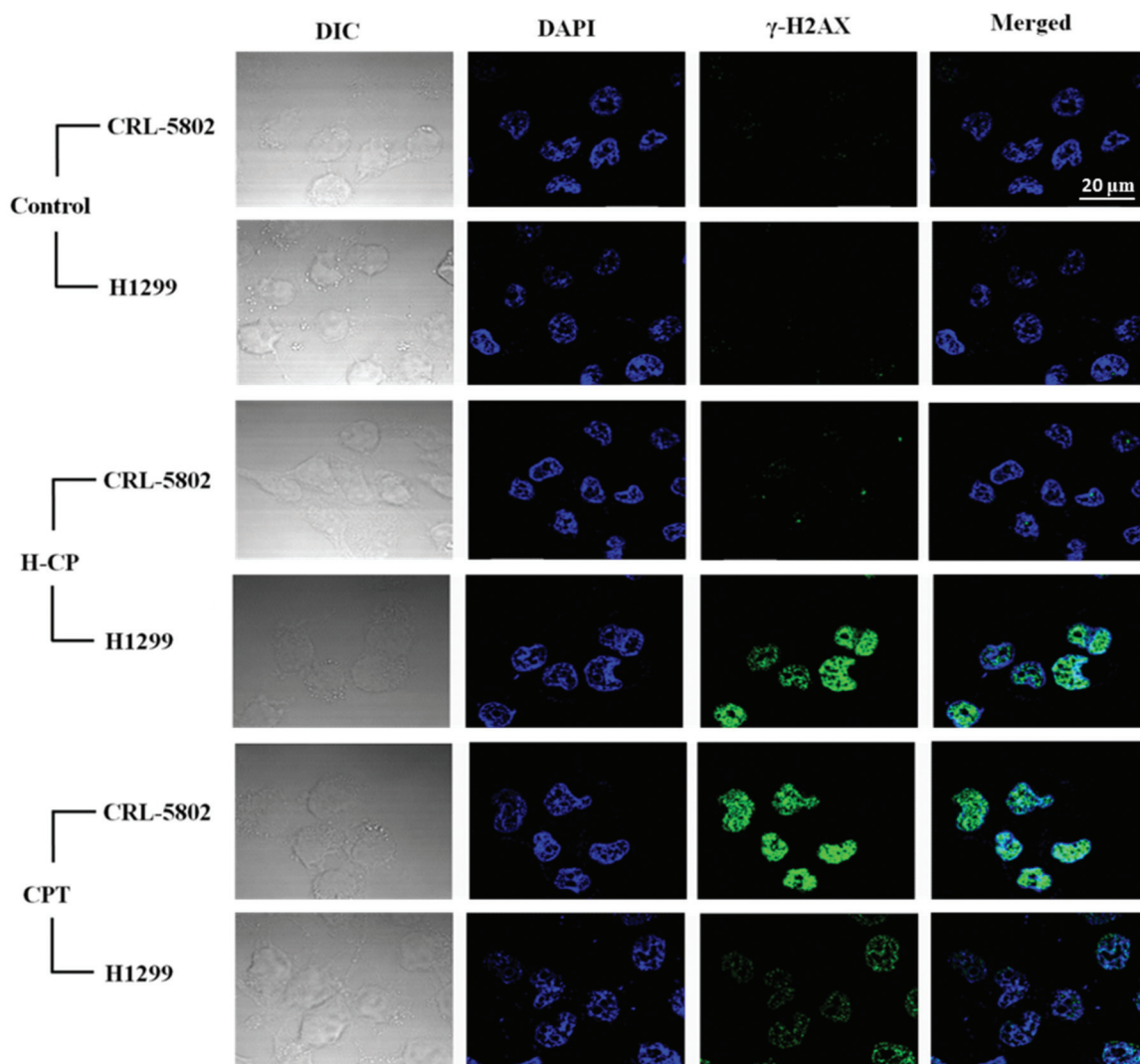


Fig. 7 CLSM images of γ -H2AX in CRL-5802 and H1299 exposed to micelle, free CPT, and micelle/CPT for 2 h of incubation using the equivalent CPT concentration of $0.1 \mu\text{g mL}^{-1}$. The cell nuclei were stained with DAPI (blue color) and γ -H2AX was stained with *p*-histone H2AX (Ser 139) monoclonal primary antibody and Alexa Fluor 488-tagged secondary antibody. The formation of γ -H2AX foci is indicated by the green fluorescence.

antibody specific for γ -H2AX and the expression of γ -H2AX was determined using flow cytometry, western blot analysis, and CLSM of cells exposed to H-CP, CPT, or micelle/CPT. As seen in the flow cytometric diagrams, the expression of γ -H2AX was very high in both cell lines exposed to CPT and micelle/CPT compared with the control group and the H-CP-treated group (Fig. 6A and B). In the CRL-5802 cells, it was much clearer that the micelle/CPT-treated cells induced a significantly higher level of γ -H2AX expression than the CPT-treated cells. When the expression of γ -H2AX in the micelle/CPT-treated cells was quantified, around a three-fold increase in γ -H2AX expression was found in the CRL-5802 cells compared with that in H1299 cells (Fig. 6B). Similar results were obtained from the western blot image (Fig. 6C), illustrating higher γ -H2AX expression in the CRL-5802 cells than in the H1299 cells. Table 1 summarizes the *in vitro* anticancer superiority of CRL-5802 cells over that of H1299 cells when the cells were exposed to micelle/CPT.

Fig. 7 shows the expression of γ -H2AX evaluated by CLSM. No γ -H2AX expression was found in the nuclei of untreated CRL-5802 and H1299 cells, slightly visible expression in cells treated with empty H-CP, and highly visible expression in cells treated with CPT and micelle/CPT. Both CPT and micelle/CPT had a higher ability to cause DNA damage in the CRL-5802 cells than in the H1299 cells because the higher intensity of green fluorescence indicates a higher expression of γ -H2AX in the nucleus.

In vivo biodistribution

To evaluate the *in vivo* accumulation of micelles in the CRL-5802 and H1299 xenografted tumors, a near-IR dye, IR780, was encapsulated into the micelles. The biodistribution of the micelle/IR780 was monitored by non-invasive fluorescence in tumor-bearing mice with the tumor grafted on the right (H1299) and left (CRL-5802) hind legs. After the tumors

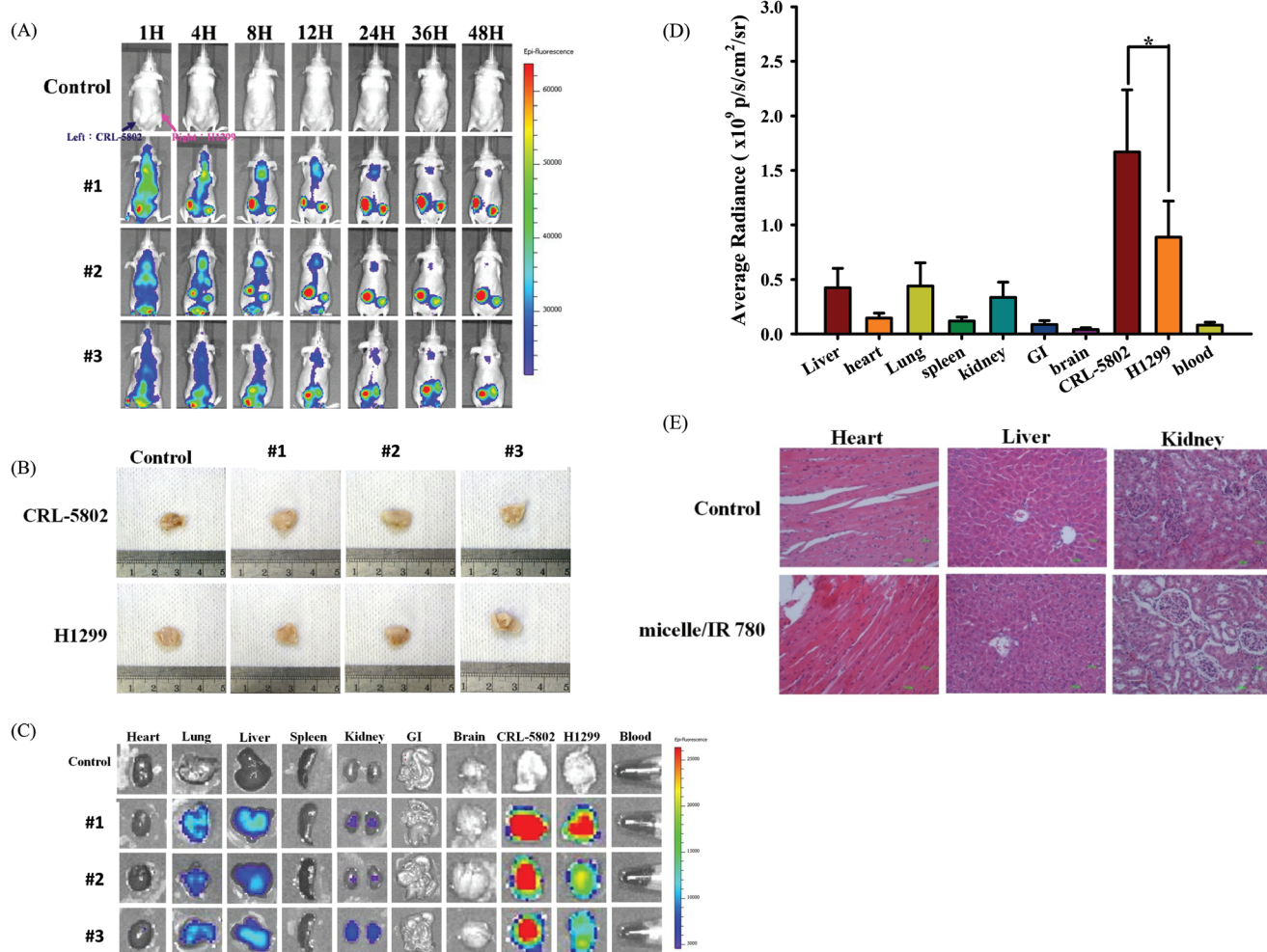


Fig. 8 (A) Optical images of CRL-5802 and H1299 tumors xenografted in male Balb/c mice (about 6 weeks old, $n = 3$, labeled as #1, 2, and 3) using a near-infrared non-invasive optical imaging technique. (B) Tumors isolated to validate similar sizes. (C) Fluorescent images and (D) relative fluorescence intensities of isolated tissues after mice were injected with the IR-780-loaded micelle (micelle/IR 780) for 48 h. (E) H&E images of the effect of the micelle on heart, liver, and kidney. The equivalent concentration of IR780 was 1.75 mg kg^{-1} using excitation and emission wavelengths of 745 and 840 nm.

had grown to approximately 150 mm³ in volume, the micelle/IR780 was intravenously injected *via* the lateral tail vein.¹⁴ After the injection, the micelle/IR780 was imaged at different time points (Fig. 8A). The fluorescence intensity of IR780 at both tumor sites increased with increasing circulation time. It was clear that the fluorescence intensity was always higher on the CRL-5802 tumor than on the H1299 tumor in mice if they were compared at the same time points. To confirm whether the higher accumulation of the micelle/IR780 on the CRL-5802 tumor was due to different tumor sizes, the tumors were isolated after 48 h. Fig. 8B clearly illustrates tumors of similar sizes. The relevant organs, tissues, and tumors from the mice were dissected 48 h after instillation and immediately optically imaged to determine the remaining fluorescence intensity. Fig. 8C shows the high IR780 fluorescence intensities at both tumor sites resulting from the EPR effect.³⁸ The optical imaging intensity of the CRL-5802 tumor was significantly higher than that of the H1299 tumor (Fig. 8D), indicating that the CRL-5802 tumor had a higher ability to internalize the micelle. To evaluate the safety of the H-CP micelle *in vivo*, the heart, liver, and kidney were harvested for histopathological examination with H&E staining. Neither noticeable organ damage nor inflammation was observed in the micelle/IR780 group compared with the saline group (Fig. 8E).

Conclusions

This study has demonstrated why lower CD44-expressing CRL-5802 cells showed higher DNA damage and higher cellular uptake than higher CD44-expressing H1299 cells when exposed to CPT or micelle/CPT. Endocytic chemical inhibitors were utilized to examine the internalization pathways of the micelle/CPT into the cells. The CRL-5802 cells involved CD44-, clathrin-, and caveolae-mediated pathways, whereas the H1299 cells involved only CD44- and caveolae-mediated pathways. Using CME seems to be superior because the micelles encapsulated with endosomes could reach the acidic lysosomes, where the abundance of enzymes helped to degrade the H-CP micelle and accelerated the release of CPT. From the cell cycle analysis of the CPT-treated cells, the CRL-5802 cells arrested mainly in the S phase and the H1299 cells mainly arrested in the G₂-M phase. The qualitative and/or quantitative evaluation of γ -H2AX expression, a biomarker for DNA damage, was obtained from flow cytometry, CLSM, and western blot studies. All the results demonstrated that the CRL-5802 cells had a higher γ -H2AX expression than the H1299 cells. The *in vivo* biodistribution of micelle/IR780 in tumor-bearing mice showed that the CRL-5802 tumor had a higher fluorescence intensity than the H1299 tumor. It can be concluded that the therapeutic outcome of a drug does not only correlate with the amount of CD44 on the surface of cancer cells. The cells used multiple internalization pathways and arrested in the S phase, as demonstrated in the CRL5802 cells, showing a higher ability to cause cell death than the H1299 cells.

Acknowledgements

We are grateful for financial support from the Ministry of Science and Technology of Taiwan (MOST103-2325-B-037-001 and MOST103-2320-B-037-012-MY3). This study was also supported by the Aim for the Top 500 Universities Grant (KMU-DT103007) and by the NSYSU-KMU Joint Research Project (NSYSUKMU 104-P026) from Kaohsiung Medical University. We appreciate the experimental support of a confocal laser scanning microscope and an optical imaging system from the Center for Research Resources and Development of KMU.

References

- 1 F. Li and K. Na, *Biomacromolecules*, 2011, **12**, 1724–1730.
- 2 F. Ronca, L. Palmieri, P. Panicucci and G. Ronca, *Osteoarthritis Cartilage*, 1998, **6**(Suppl A), 14–21.
- 3 R. Bagari, D. Bansal, A. Gulbake, A. Jain, V. Soni and S. K. Jain, *J. Drug Targeting*, 2011, **19**, 251–257.
- 4 D. Naor, R. V. Sionov and D. Ish-Shalom, in *Adv. Cancer Res.*, ed. F. V. W. George and K. George, Academic Press, 1997, vol. 71, pp. 241–319.
- 5 H. A. Kargi, M. F. Kuyucuoglu, M. Alakavuklar, O. Akpinar and S. Erk, *Cancer Lett.*, 1997, **119**, 27–30.
- 6 Y. S. Liu, C. C. Chiu, H. Y. Chen, S. H. Chen and L. F. Wang, *Mol. Pharm.*, 2014, **11**, 1164–1175.
- 7 O. M. Koo, I. Rubinstein and H. Onyuksel, *Nanomedicine*, 2005, **1**, 77–84.
- 8 Q. Y. Li, Y. G. Zu, R. Z. Shi and L. P. Yao, *Curr. Med. Chem.*, 2006, **13**, 2021–2039.
- 9 E. K. Park, S. B. Lee and Y. M. Lee, *Biomaterials*, 2005, **26**, 1053–1061.
- 10 G. Pasut and F. M. Veronese, *Adv. Drug Delivery Rev.*, 2009, **61**, 1177–1188.
- 11 X. Y. Zhu, X. Z. Zhang, L. Xu, X. Y. Zhong, Q. Ding and Y. X. Chen, *Biochem. Biophys. Res. Commun.*, 2009, **379**, 1084–1090.
- 12 S. F. Peng, C. J. Su, M. C. Wei, C. Y. Chen, Z. X. Liao, P. W. Lee, H. L. Chen and H. W. Sung, *Biomaterials*, 2010, **31**, 5660–5670.
- 13 C.-C. Chiu, J.-W. Haung, F.-R. Chang, K.-J. Huang, H.-M. Huang, H.-W. Huang, C.-K. Chou, Y.-C. Wu and H.-W. Chang, *PLoS One*, 2013, **8**, e64739.
- 14 C. L. Peng, Y. H. Shih, P. C. Lee, T. M. Hsieh, T. Y. Luo and M. J. Shieh, *ACS Nano*, 2011, **5**, 5594–5607.
- 15 G. Sahay, D. Y. Alakhova and A. V. Kabanov, *J. Controlled Release*, 2010, **145**, 182–195.
- 16 O. Harush-Frenkel, N. Debotton, S. Benita and Y. Altschuler, *Biochem. Biophys. Res. Commun.*, 2007, **353**, 26–32.
- 17 W. Li, C. Chen, C. Ye, T. Wei, Y. Zhao, F. Lao, Z. Chen, H. Meng, Y. Gao, H. Yuan, G. Xing, F. Zhao, Z. Chai, X. Zhang, F. Yang, D. Han, X. Tang and Y. Zhang, *Nanotechnology*, 2008, **19**, 145102.

- 18 J. Z. Rappoport, *Biochem. J.*, 2008, **412**, 415–423.
- 19 P. J. Smith, M. Giroud, H. L. Wiggins, F. Gower, J. A. Thorley, B. Stolpe, J. Mazzolini, R. J. Dyson and J. Z. Rappoport, *Int. J. Nanomed.*, 2012, **7**, 2045–2055.
- 20 G.-J. Chen, C. Hsu, J.-H. Ke and L.-F. Wang, *J. Biomed. Nanotechnol.*, 2015, **11**, 951–963.
- 21 O. Harush-Frenkel, E. Rozentur, S. Benita and Y. Altschuler, *Biomacromolecules*, 2008, **9**, 435–443.
- 22 L. Qiu, Z. Li, M. Qiao, M. Long, M. Wang, X. Zhang, C. Tian and D. Chen, *Acta Biomater.*, 2014, **10**, 2024–2035.
- 23 M. E. Wall, M. C. Wani, C. E. Cook, K. H. Palmer, A. T. McPhail and G. A. Sim, *J. Am. Chem. Soc.*, 1966, **88**, 3888–3890.
- 24 J. A. Seiler, C. Conti, A. Syed, M. I. Aladjem and Y. Pommier, *Mol. Cell. Biol.*, 2007, **27**, 5806–5818.
- 25 F. Goldwasser, T. Shimizu, J. Jackman, Y. Hoki, P. M. O'Connor, K. W. Kohn and Y. Pommier, *Cancer Res.*, 1996, **56**, 4430–4437.
- 26 J. Fueyo, C. Gomez-Manzano, V. Puduvalli, P. Martin-Duque, R. Perez-Soler, V. Levin, W. Yung and A. Kyritsis, *Int. J. Oncol.*, 1998, **12**, 665–674.
- 27 W. A. Cliby, K. A. Lewis, K. K. Lilly and S. H. Kaufmann, *J. Biol. Chem.*, 2002, **277**, 1599–1606.
- 28 Z. Darzynkiewicz, S. Bruno, G. Del Bino and F. Traganos, *Ann. N. Y. Acad. Sci.*, 1996, **803**, 93–100.
- 29 A. J. Ryan, S. Squires, H. L. Strutt and R. T. Johnson, *Nucleic Acids Res.*, 1991, **19**, 3295–3300.
- 30 K. Avemann, R. Knippers, T. Koller and J. M. Sogo, *Mol. Cell. Biol.*, 1988, **8**, 3026–3034.
- 31 Y.-P. Tsao, P. D'Arpa and L. F. Liu, *Cancer Res.*, 1992, **52**, 1823–1829.
- 32 R. A. Tobey, *Cancer Res.*, 1972, **32**, 2720–2725.
- 33 A. Martín, J. Odajima, S. L. Hunt, P. Dubus, S. Ortega, M. Malumbres and M. Barbacid, *Cancer Cell*, 2005, **7**, 591–598.
- 34 M. Zhang, J. Li, L. Wang, Z. Tian, P. Zhang, Q. Xu, C. Zhang, F. Wei and W. Chen, *Oncol. Lett.*, 2013, **6**, 381–386.
- 35 R. Vrhovac, A. Delmer, R. Tang, J.-P. Marie, R. Zittoun and F. Ajchenbaum-Cymbalista, *Blood*, 1998, **91**, 4694–4700.
- 36 W. Sterlacci, M. Fiegl, W. Hilbe, H. Jamnig, W. Oberaigner, T. Schmid, F. Augustin, J. Auberger, E. C. Obermann and A. Tzankov, *J. Thoracic Oncol.*, 2010, **5**, 1325–1336.
- 37 J. Dickey, C. Redon, A. Nakamura, B. Baird, O. Sedelnikova and W. Bonner, *Chromosoma*, 2009, **118**, 683–692.
- 38 H. Maeda and Y. Matsumura, *Adv. Drug Delivery Rev.*, 2011, **63**, 129–130.